© 2020. Published by The Company of Biologists Ltd | Journal of Cell Science (2020) 133, jcs237156. doi:10.1242/jcs.237156

RESEARCH ARTICLE

Passive diffusion through nuclear pore complexes regulates levels of the yeast SAGA and SLIK coactivator complexes

Tadashi Makio and Richard W. Wozniak*

ABSTRACT

Nuclear pore complexes (NPCs) control gene expression by regulating the bi-directional exchange of proteins and RNAs between nuclear and cytoplasmic compartments, including access of transcriptional regulators to the nucleoplasm. Here, we show that the yeast (*Saccharomyces cerevisiae*) nucleoporin Nup170, in addition to binding and silencing subtelomeric genes, supports transcription of genes regulated by the SAGA transcriptional activator complex. Specifically, we show that a lower amount of SAGA complex is bound to target genes in the absence of Nup170. Consistent with this observation, levels of the SAGA complex are decreased in cells lacking Nup170, while those of the SAGA-related SLIK complexes are increased. This change in the ratio of SAGA to SLIK complexes is due to increased nuclear activity of Pep4, a protease responsible for production of the SLIK complex. Further analyses of various nucleoporin mutants revealed that the increased nuclear entry of Pep4 observed in the *nup170*Δ mutant likely occurs as the consequence of an increase in the sieving limits of the NPC diffusion channel. On the basis of these results, we propose that changes in passive diffusion rates represent a mechanism for regulating SAGA- and SLIK complex-mediated transcriptional events.

KEY WORDS: Nuclear pore complex, Nup170, SAGA complex, SLIK complex, Nuclear transport, Passive diffusion, Yeast

INTRODUCTION

The nuclear envelope (NE) double membrane forms an impermeable barrier between the nucleoplasm and the cytoplasm. For molecules to enter or leave the nucleus they are funneled through massive channels formed by nuclear pore complexes (NPCs), which perforate the NE at numerous positions along the surface of the nucleus. NPCs are present in all eukaryotes and their overall structural organization appears largely conserved. In the yeast *S. cerevisiae*, NPCs are ∼100 nm diameter and consist of multiple copies of ∼30 different proteins, termed nucleoporins or Nups (Aitchison and Rout, 2012). The components are categorized into several classes based on their sequence and functional features. Many of the most conserved Nups form the cylindrical scaffold of the NPC, while a second group, each rich in the phenylalanine-glycine repeat-containing peptides (FG-Nups), line the transport channel and extend into the cytoplasm and nucleoplasm (Aitchison and Rout, 2012).

There are two mechanisms by which molecules move through the NPC: facilitated and passive diffusion. Facilitated diffusion is mediated by nuclear transport factors (NTFs). NTFs contain multiple binding interfaces that allow them to bind nuclear import or export signals in transport cargos as well as the FG-Nups. Interactions of the NTFs with the FG-Nups are generally of low affinity, allowing NTFs and their attached cargos to partition into and out of the NPC channel without an appreciable change in free energy (Rout et al., 2003; Wente and Rout, 2010). Once in the channel, the NTF–cargo complex can diffuse into either cytoplasm or nucleoplasm (Lowe et al., 2010). This process allows cargos of a broad range of sizes to pass through NPCs. Directionality of transport (i.e. import or export) is then established by additional factors (e.g. RanGTP) that bind and cause the NTF–cargo complexes to dissociate in the target compartment (Aitchison and Rout, 2012).

Macromolecules lacking nuclear transport signals are also able to enter the nucleus by passive diffusion, but their movement through NPCs is limited by their size. Classical studies using inert dextrans and labeled proteins concluded that NPCs contained a passive channel of 4.5–5.9 nm in radius that would allow molecules up to ∼40–60 kDa in mass to diffuse through NPCs (Peters, 1983; Paine, 1975; Paine and Feldherr, 1972). Numerous follow up studies supported these conclusions. However, other studies have suggested the passive channel could accommodate larger molecules (Wang and Brattain, 2007; Popken et al., 2015). These observations called into question previous assumptions that the passive diffusion channel was rigid, with a defined size threshold. Importantly, a recent study showed that the passive diffusion channel is unlikely to be rigid (Timney et al., 2016). Instead, these authors proposed that the channel is flexible and capable of allowing passive diffusion of much larger molecules than previously assumed, at rates that decrease with increasing mass. Consistent with this conclusion, analysis of the vertebrate nuclear and cytoplasmic proteome has revealed many proteins and protein complexes of up to ∼100 kDa are equally distributed in both compartments suggesting they partition across the NE (Wühr et al., 2015). The molecular characteristics of the channel that establish and regulate passive diffusion properties are currently unclear. However, what is known is that several FG-Nups present within the central channel of the NPC (Hülsmann et al., 2012; Popken et al., 2015; Timney et al., 2016) and Nups present within the inner ring complex, namely Nup170 and Nup188 (Shulga et al., 2000), are required for maintaining the permeability properties of the passive diffusion channel.

By regulating macromolecular transport, NPCs directly influence the contents of the nucleoplasm and essentially all nuclear processes. Principal among these is transcription of mRNA. Many components of the transcriptional machinery contain nuclear localization signals (NLSs) and they have been shown, or assumed, to be imported into the nucleus by NTFs. However, passive diffusion is also likely to contribute to transcriptional control. For example, increases in the mass threshold for passive diffusion through NPCs have been reported to occur in response to

Department of Cell Biology, University of Alberta, Edmonton, AB, Canada, T6G 2H7.

*Author for correspondence (rick.wozniak@ualberta.ca)

R.W.W., 0000-0003-2328-0247

Received 5 August 2019; Accepted 31 January 2020

Journal of Cell Science (2020) 133, jcs237156. doi:10.1242/jcs.237156

stress or as cells age (D'Angelo et al., 2009; Mason et al., 2005), and these changes are accompanied by alterations in transcription (López-Otín et al., 2013). A hypothesis arising from these observations is that changes in passive diffusion offer a potential mechanism for globally regulating transcription and potentially other nuclear functions. However, what pathways and specific molecular events might be altered in response to changes in passive diffusion remains to be determined.

The impact of Nups on gene expression extends beyond their roles on regulating transport. Various Nups have been shown to interact with chromatin and influence the transcriptional status of resident genes. In certain cases Nups, including several FG-Nups, have been shown to interact with and assist in the assembly of transcription machinery on actively transcribed genes (Ptak et al., 2014; Ptak and Wozniak, 2016; Ibarra and Hetzer, 2015). In other instances, Nups can play a repressive role (Therizols et al., 2006; Van De Vosse et al., 2013). For example, yeast Nup170 interacts with subtelomeric chromatin, and this association is required for the assembly of silencing factors on chromatin and the repression of resident subtelomeric genes (Van De Vosse et al., 2013). As these varied functions of Nups would imply, the consequences of loss-of-function mutations of a given Nup on gene expression are a product of both direct effects on chromatin structure and indirect effects arising from alteration of the nuclear transport pathway discussed above. Thus, it is important to consider that transcriptional changes observed for a given *nup* mutation are an amalgamation of changes caused by the loss of multiple functions of that Nup. For example, our previous analysis of cells lacking Nup170 showed that the majority of genes affected showed an increase in expression, and many of these were detected in regions of the genome that bound Nup170 (Van De Vosse et al., 2013). However, a smaller group of genes showed a decrease in expression suggesting an alternative function for Nup170 in regulating their expression.

Here, we have investigated the mechanism by which Nup170 supports the transcription of a group of genes controlled by Spt–Ada–Gcn5 acetyltransferase (SAGA) coactivator complex in the yeast *Saccharomyces cerevisiae*. We observed that representative genes within this group show reduced levels of associated SAGA complex in the absence of Nup170. Consistent with these data, cellular levels of SAGA complex were also lower, while those for a related complex, the SAGA-like (SLIK) complex, were increased. We show that this change in the ratio of SAGA to SLIK complexes in the *nup170*Δ mutant is due to increased nuclear activity of Pep4, a protease responsible for production of the SLIK complex. Our further analyses lead us to propose that the increased nuclear levels of Pep4 observed in the *nup170*Δ mutant occur as a consequence of increased passive diffusion through NPCs. On the basis of our observations, we propose that changes in passive diffusion rates through NPCs, which can arise as a consequence of changes in cell physiology, represent a mechanism for globally modulating nuclear functions, including the regulation of SAGA- and SLIK complex-mediated transcriptional events.

RESULTS

Expression of SAGA complex target genes is decreased in *nup170*Δ cells

In a previous study, we found that the gene expression pattern of yeast cells lacking the NPC protein Nup170 showed specific alterations (Van De Vosse et al., 2013). Notably many genes within subtelomeric chromatin regions were upregulated. However, a subset of genes positioned throughout the genome exhibited reduced mRNA levels. Further inspection of these genes revealed an enrichment of genes regulated by the SAGA transcriptional coactivator complex (Fig. S1). The SAGA complex contains multiple functional groups, including a histone acetyltransferase, that function to support the transcription of ∼10% of the genes transcribed by RNA polymerase II (Pol II) (Huisinga and Pugh, 2004; see Fig. S1). Genes in this category, referred to as SAGA-dominated genes, are overrepresented among those downregulated in the *nup170*Δ mutant, where 38 genes out of the top 100 most downregulated genes are categorized as SAGA-dominated genes (P=6×10^{-25} on the Pearson's χ-squared test).

Levels of mRNAs encoded by SAGA-dominated genes in the *nup170*Δ mutant were further confirmed by quantitative (q)PCR. Analysis of selected SAGA-dominated genes, including *PHO5*, *PDR5* and *HIS4*, showed reduced mRNA levels in the *nup170*Δ mutant, while expression levels of several transcription factor IID (TFIID)-dominated genes, including genes such as *DPS1* and *SUR4*, showed no significant change relative to the wild-type (WT) controls (Fig. 1A). Consistent with changes in mRNA levels of SAGA-dominated genes, we also observed a reduction in RNA Pol II density on these genes in the *nup170*Δ mutant. A chromatin immunoprecipitation (ChIP) experiment using antibodies against the RNA Pol II component Rpb3 was performed to examine RNA Pol II density along two SAGA-dominated genes, *HIS4* and *PDR5*, showing reduced transcripts in the *nup170*Δ mutant. As shown in Figs 1B and 2B, the enrichment of RNA Pol II at the *HIS4* and *PDR5* gene loci was reduced in the *nup170*Δ mutant, suggesting RNA Pol II association with these SAGA-dominated genes was defective. By contrast, two TFIID-dominated genes, *RPL3* and *DPS1*, whose transcript levels were not reduced in the *nup170*Δ mutant, show similar levels of RNA Pol II enrichment in the WT and *nup170*Δ mutant strains (Fig. 1B). These results suggest that transcription of the *HIS4* and *PDR5* genes, and likely additional SAGA-dominated genes, is compromised in cells lacking Nup170.

Preinitiation complex association with SAGA-dominated gene promoters is defective in the *nup170*Δ mutant

To further understand the functional basis for the attenuated transcription of genes in the absence of Nup170, we examined the consequences of Nup170 loss on assembly of the preinitiation complex (PIC), including components of the SAGA complex, RNA Pol II, transcriptional activators and histones, at promoter regions of several SAGA-dominated genes that show varying degrees of reduced expression in *nup170*Δ mutant – *SNQ2* (0.80 fold), *PDR5* (0.39 fold) and *HIS4* (0.35 fold) (Fig. 1A and Van De Vosse et al., 2013). ChIP analysis was employed to examine the association of Hfi1 (a SAGA complex protein), Rpb3, histone H3, and the transcriptional activators Pdr1 and Bas2 to the promoter regions of *PDR5*, *SNQ2* and *HIS4* in the WT and *nup170*Δ mutant strains. As shown in Fig. 2B, in WT cells, we detected the enrichment of Hfi1 and Rpb3 at the promoter regions of *PDR5*, *SNQ2* and *HIS4*. Importantly, these interactions were significantly reduced in strains lacking Nup170 (Figs 1B and 2B). We also examined the association of two transcriptional activators with the three target genes – Bas2 binding to *HIS4*, and Pdr1 binding to *PDR5* and *SNQ2*. We observed that, in the absence of Nup170, binding of Bas2 to the promoter region of *HIS4* was significantly reduced. Similarly, a smaller, but significant, reduction in the association of Pdr1 was detected with *PDR5* promoter region, while the binding of Pdr1 to *SNQ2* appeared unchanged (Fig. 2B).

Histone association with the promoter regions also provides an indication of the transcriptional state of genes, as they are generally excluded from the promoter regions of transcribing genes (Hartley

Journal of Cell Science (2020) 133, jcs237156. doi:10.1242/jcs.237156

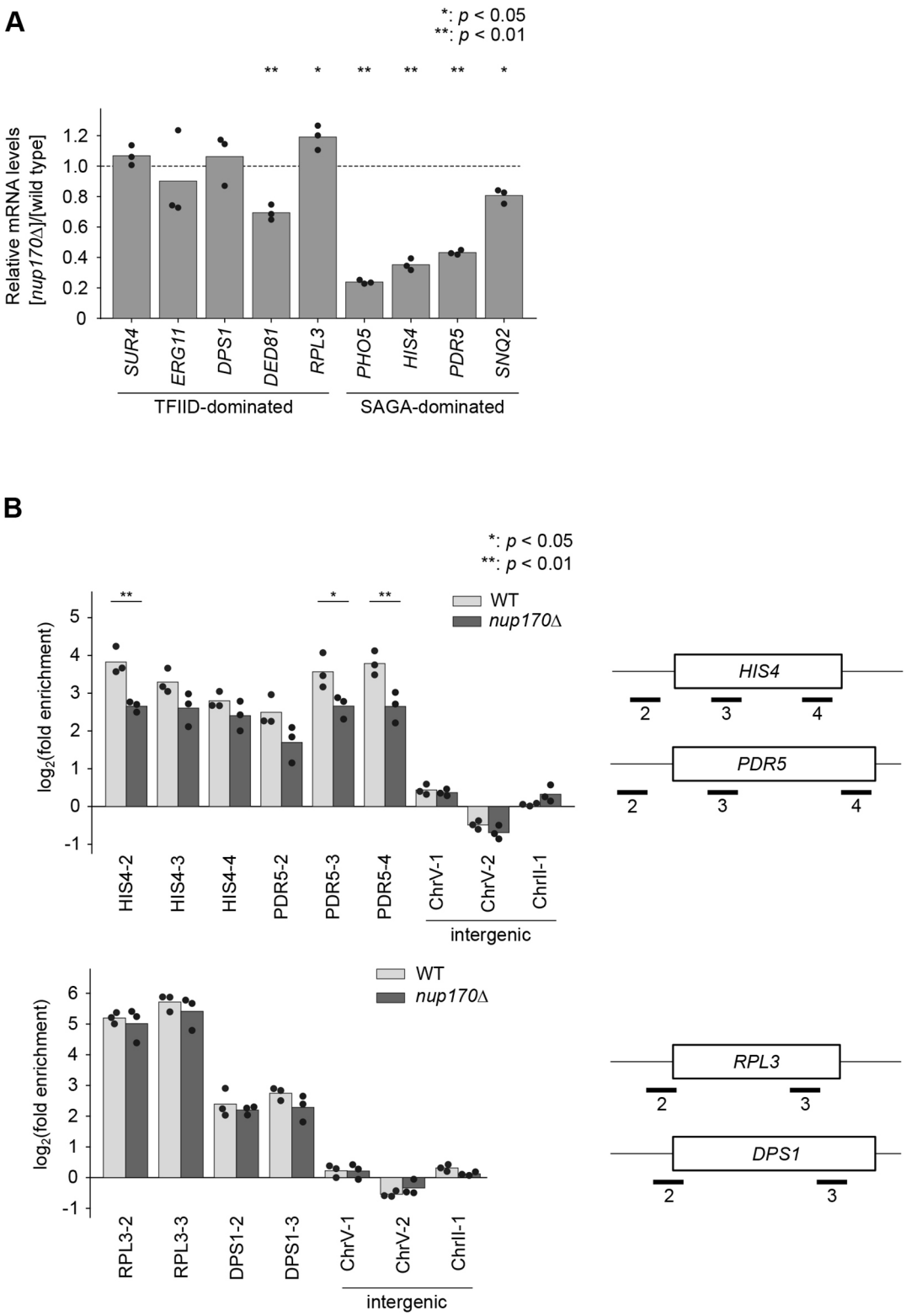

Fig. 1. Loss of Nup170 preferentially suppresses expression of genes regulated by the SAGA coactivator complex. (A) The fold change in mRNA levels of the indicated genes in the *nup170*Δ mutant compared with the WT strain were examined by qPCR. The genes are categorized as either TFIID or SAGA dominated (Huisinga and Pugh, 2004; Barbaric et al., 2003). Individual observations are plotted as filled circles (n=3). The genes whose mRNA level was significantly altered in the *nup170*Δ mutant are marked with asterisks (two-tailed paired t-test). (B) The RNA Pol II density on various genes was examined by ChIP analysis using an anti-Rpb3 antibody. The enrichment of genomic regions was quantified by qPCR, and normalized with that of the intergenic regions (ChrV-1, ChrV-2 and ChrII-1). The regions amplified in the qPCR relative to the ORFs (indicated by boxes) are shown to the right of the plots. Region 2 for each gene includes the transcription start site, and regions 3 and 4 are located within the ORF. The individual observations are plotted as filled circles (n=3) on a $\log_2$ scale. The regions showing significant difference in enrichment between the WT and the *nup170*Δ mutant, as determined by a two-tailed Student's t-test, are marked with asterisks.

Journal of Cell Science (2020) 133, jcs237156. doi:10.1242/jcs.237156

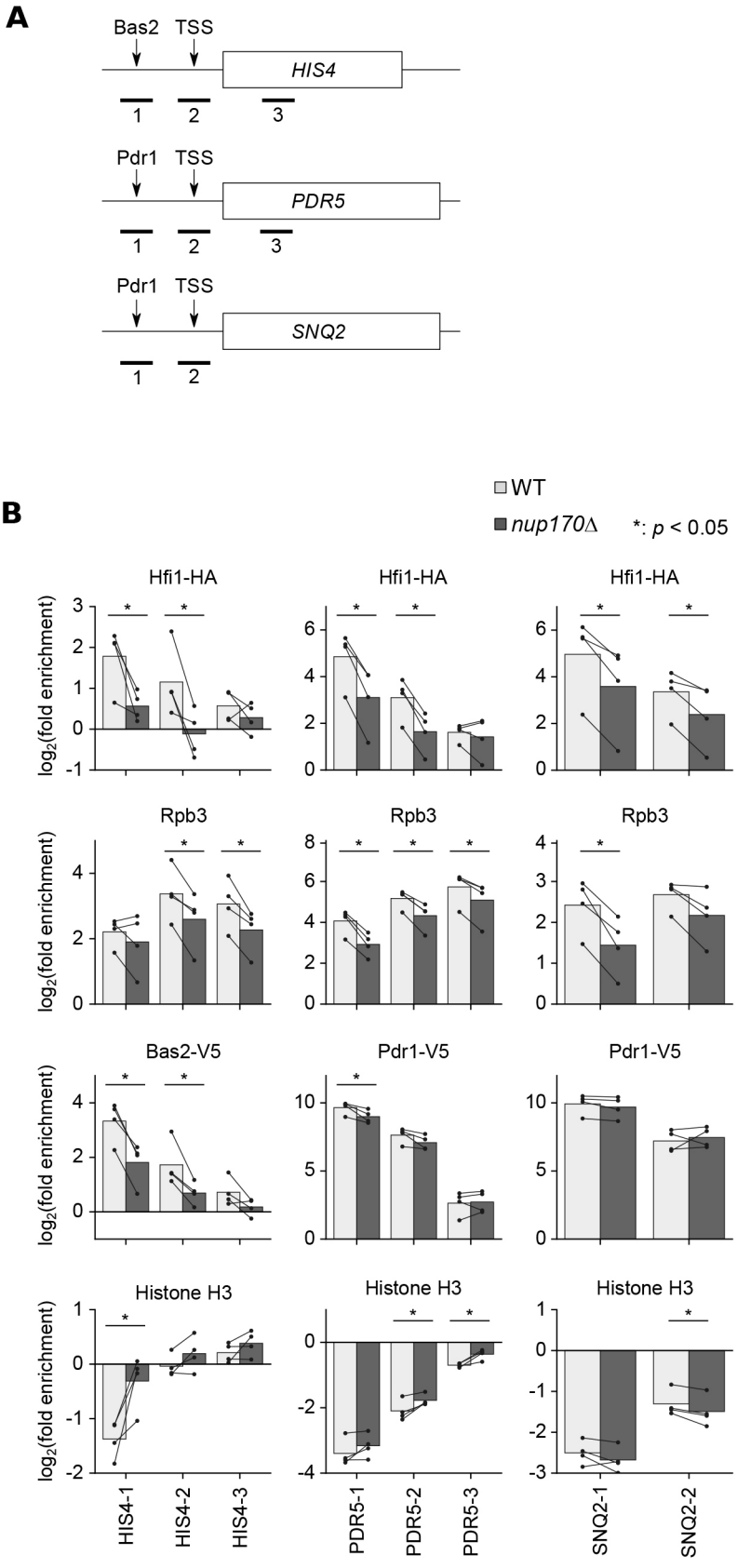

Fig. 2. Genes repressed in the *nup170*Δ mutant exhibit reduced association of preinitiation complex components. (A) ChIP analysis was performed using primer sets that detect the indicated regions of *HIS4*, *PDR5* and *SNQ2*. The locations of these regions are shown in the schematic diagram. Region 1 for each gene includes the binding sites for the gene-specific transcriptional activator (Bas2 or Pdr1). Region 2 includes the transcriptional start site (TSS). Region 3 is located within the ORF. (B) WT and the *nup170*Δ mutant strains producing Hfi1–HA and either of Pdr1–V5 or Bas2–V5 were subjected to ChIP analysis using antibodies directed against the V5 or HA tags, Rpb3 and histone H3. The enrichment of the genomic regions was quantified using qPCR and normalized as described in Fig. 1B. The individual observations are plotted as filled circles (n=4) on a $\log_2$ scale, and the data points from each repeated experiment are connected with a line. Regions showing significant differences in enrichment between the WT and the *nup170*Δ strain, as determined using a two-tailed paired *t*-test, are marked with asterisks.

and Madhani, 2009). We confirmed this using ChIP analysis in the WT strain by showing that the promoter regions of *PDR5*, *SNQ2* and *HIS4* were less enriched for histone H3 than the non-transcribed (background) regions (Fig. 2B). By contrast, in the *nup170*Δ mutant, histone occupancy at the *HIS4* promoter region was significantly increased, consistent with its reduced transcription. For

Journal of Cell Science (2020) 133, jcs237156. doi:10.1242/jcs.237156

PDR5, similar alterations were detected but were less substantial, while *SNQ2* showed little or no change (Fig. 2B). Notably, in the *nup170*Δ mutant, the greater increases in histone occupancy associated with the *HIS4* and *PDR5* loci, as compared to the *SNQ2* locus, correlated with greater decreases in the expression of the *HIS4* and *PDR5* as compared to *SNQ2* (see Figs 1A and 2B).

Nup170 regulates cellular levels of the SAGA complex component Spt7

Our observations that numerous SAGA-dominated genes show reduced expression in the *nup170*Δ mutant led us to investigate how the loss of Nup170 altered the SAGA complex. In order to examine the composition of the SAGA complex, we affinity purified the SAGA complex from WT and the *nup170*Δ mutant cells using a TAP-tagged version of the SAGA core component Spt20 (Spt20–TAP). Similar groups of proteins were isolated from WT and *nup170*Δ mutant cell extracts, and both displayed a banding pattern after SDS-PAGE similar to that previously reported for the Spt20–TAP-associated SAGA complex (see Spedale et al., 2010; also see Table S1). However, a reproducible difference between WT and *nup170*Δ preparations was detected in the relative abundance of three protein species with apparent masses of ∼80 kDa, ∼180 kDa and ∼200 kDa (Fig. 3A). Specifically, Spt20–TAP-associated proteins derived from the *nup170*Δ mutant showed reduced amounts of the 80 kDa and 200 kDa polypeptides, and increased levels of the 180 kDa species (Fig. 3A). Previous analysis of the Spt20–TAP purified SAGA complex had identified the corresponding proteins as Spt8 (80 kDa), Spt7 (200 kDa) and a C-terminal truncation of Spt7 (180 kDa) (Spedale et al., 2010). Consistent with these results, our mass spectrometry analysis of Spt20–TAP purified SAGA components identified Spt7 as the prominent species at 180 kDa and 200 kDa, and the presence of Spt8 at 80 kDa (see Table S2). In regions of the gel containing the 180 kDa and 200 kDa proteins, lower levels of peptides derived from Tra1 were also detected, likely arising from degradation products of this ∼430 kDa component of the SAGA complex (Table S2). The 200 kDa species likely contains full-length Spt7, as peptides from the entire length of Spt7 were detected in this region of the gel. By contrast, the 180 kDa species is likely a C-terminal truncation of Spt7, as no peptides after amino acid residue 938 were detected in this band (Table S3).

The C-terminal truncation of Spt7 has been previously shown to arise from the specific cleavage of Spt7 by vacuolar protease Pep4 following residue 1141 (Spedale et al., 2010; Mischerikow et al., 2009). To assess the role of Pep4 in the increased cleavage of Spt7 observed in the *nup170*Δ mutant, strains were constructed containing an Spt7–TAP fusion protein. In WT cells, full-length and proteolytic fragments of Spt7–TAP were visible by western blotting, including a polypeptide with molecular mass approximating the predicted 50 kDa size of the Pep4-produced C-terminal Spt7–TAP fragment (CT-Spt7–TAP; Fig. 3B). Importantly, we observed that the amount of the CT-Spt7–TAP fragment was increased in the *nup170*Δ mutant (see Fig. 3B, lanes 2 and 4; Fig. 3C), and its presence in WT and the *nup170*Δ mutant was dependent on Pep4 (Fig. 3B; see *pep4*Δ and *nup170*Δ *pep4*Δ). Consistent with these results, we also observed a decrease in the amount of full-length Spt7–TAP in the *nup170*Δ mutant, which was also Pep4 dependent. This decrease in full-length Spt7–TAP was not as apparent (in western blots) in the WT strain as compared to the *pep4*Δ mutant, likely due to a smaller fraction of Spt7–TAP pool being cleaved in WT cells. On the basis of these results, we conclude that the increased cleavage of Spt7 in the *nup170*Δ mutant is Pep4 dependent.

The C-terminal truncation of Spt7 is associated with a SAGA-like (SLIK) coactivator complex that lacks Spt8 (Pray-Grant et al., 2002; Sterner et al., 2002; see Table S1). Given that core subunits, such as Spt20, are components of both SAGA and SLIK, purification of Spt20–TAP reveals a ratio of full-length Spt7 (∼200 kDa) to its C-terminal truncation (∼180 kDa) that reflects the *in vivo* ratio of the SAGA and SLIK complexes. In the *nup170*Δ mutant, the increased amount of the Spt7 C-terminal truncation bound to purified Spt20–TAP suggests both increased Pep4-dependent cleavage of Spt7 and a corresponding elevation in levels of SLIK. Consistent with this conclusion, our results revealed a reduction of Spt8–Myc bound to Spt20–TAP purified from the *nup170*Δ mutant (Fig. 3D). These results suggest that Nup170 is required for maintaining the cellular ratio of the SAGA and SLIK complexes. This function for Nup170, however, does not appear to involve a direct interaction between Nup170 and the SAGA or SLIK complex, as we did not detect Nup170 bound to the SAGA complex (data not shown).

The NPC permeability barrier controls Pep4 accessibility to the nucleoplasm

Pep4 is a vacuolar protease that is processed to an active form in the lumen of the vacuole. Pep4-dependent cleavage of Spt7 is presumed to occur following the movement of some portion of active Pep4 from the vacuole lumen to the nucleoplasm. While the mechanism by which Pep4 crosses the vacuolar membrane is undefined, it has been proposed that, once in the cytoplasm, Pep4 enters the nucleoplasm (Spedale et al., 2010). Pep4 does not contain a canonical NLS, but its molecular mass (43 kDa) would permit it to passively diffuse through NPCs and into the nucleoplasm (Timney et al., 2016). Importantly, NPCs lacking Nup170 exhibit significantly elevated permeability, with various reporter proteins (up to 126 kDa) showing increased equilibration rates between the nucleoplasm and cytoplasm (Shulga et al., 2000; Timney et al., 2016). On the basis of these observations, we tested whether the loss of Nup170 would increase the accessibility of Pep4 to nuclear substrates. For these experiments, we constructed reporter substrates that are restricted to the cytoplasm or the nucleoplasm (Fig. 4A). The reporter proteins contain a segment of Spt7 (tSpt7; residues 1088–1180) that includes the Pep4 cleavage site (following residue 1141) flanked by GFP and GST. To this chimeric protein, a nuclear localization (SV40 *NLS*) or nuclear export (PKI *NES*) signal was added, which drives the accumulate of the reporter protein in the nucleoplasm (GFP–*NLS*–tSpt7–GST) or cytoplasm (GFP–*NES*–tSpt7–GST) (Fig. 4B). Western blot analysis of WT cells producing these reporters revealed both the full-length (∼70 kDa) and an ∼34 kDa cleavage fragment predicted to be produced by Pep4 (Fig. 4C). Consistent with this conclusion, the presence of the ∼34 kDa reporter cleavage fragments was dependent on Pep4 (Fig. 4C). Also of note, detection of the full-length reporters suggests the Pep4 substrates were not a limiting factor in the production of the ∼34 kDa reporter cleavage fragments. We compared the levels of the NLS and NES reporter cleavage products (each normalized to their full-length counterpart) to produce a relative ratio of NLS to NES reporter cleavage in each strain. In WT cells this ratio was ∼0.6, suggesting that cleavage of the nucleoplasmic NLS-containing reporter was less efficient than cleavage of the cytoplasmic NES-containing reporter (see Fig. 4C, lanes 1 and 2; Fig. 4D). By contrast, in the *nup170*Δ strain, we observed a significant increase in the ratio of NLS to NES reporter cleavage products to ∼1.5 (Fig. 4D). These results are consistent with the conclusion that nuclear Pep4-dependent cleavage events are increased in the *nup170*Δ strain.

Journal of Cell Science (2020) 133, jcs237156. doi:10.1242/jcs.237156

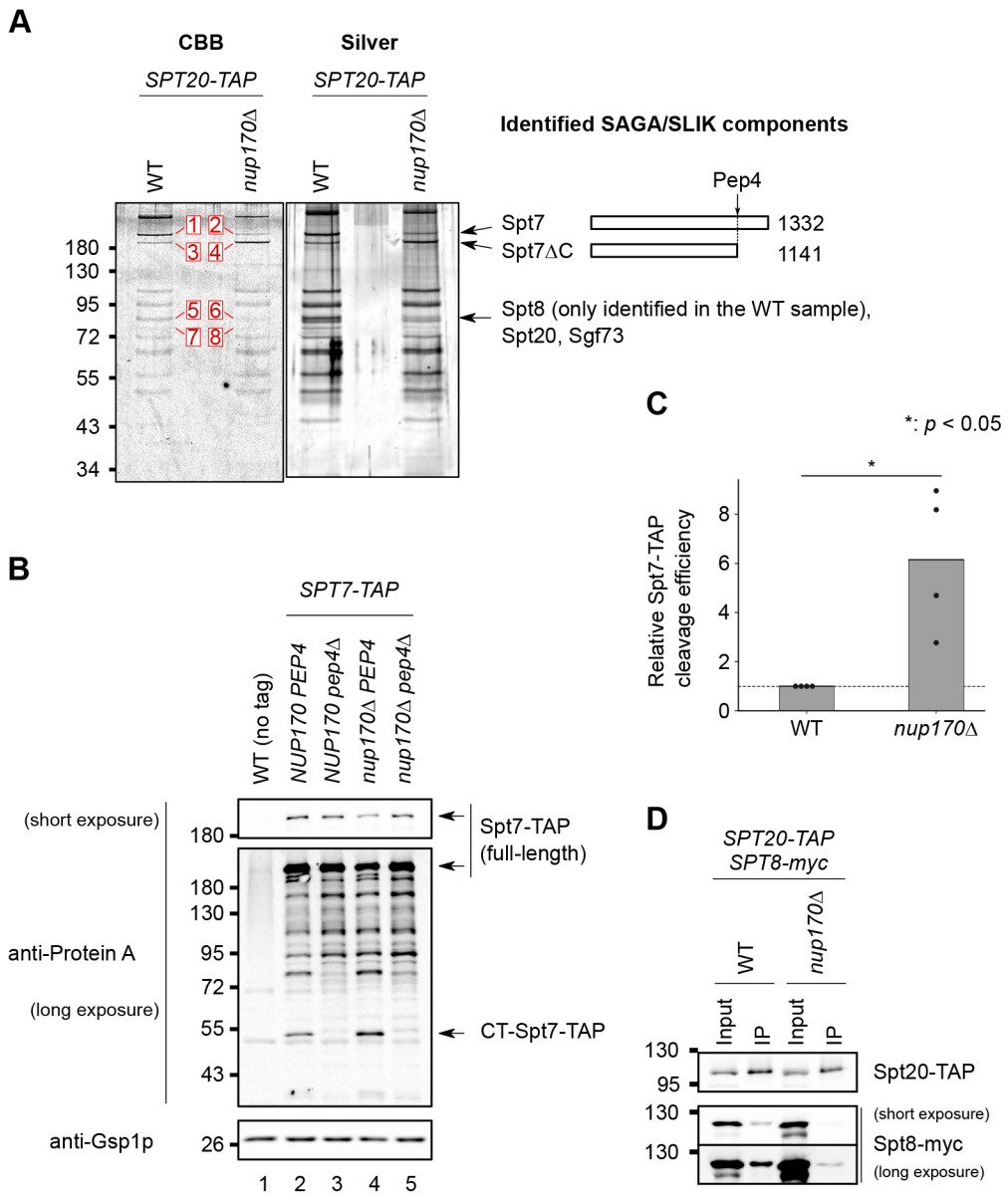

Fig. 3. Nup170 is required for maintaining the cellular ratio of the SAGA and SLIK complexes. (A) Spt20–TAP and associated proteins were purified from WT and *nup170*Δ cell lysates using IgG-conjugated Dynabeads. Protein complexes released from the beads were analyzed by SDS-PAGE followed by the CBB or Silver staining. Protein species showing apparent differences in staining intensity between WT and the *nup170*Δ mutant samples are indicated and numbered. The numbered protein species were cleaved and their peptides were analyzed by mass spectrometry. SAGA and SLIK components were identified at the positions indicated by arrows. All proteins identified by mass spectrometry analysis are shown in Table S2. (B) The whole-cell extracts were prepared from the indicated mutant cells producing Spt7–TAP, and extracts were analyzed by western blotting using anti-Protein A and anti-Gsp1 (loading control) antibodies. The protein extracts from WT cells (no tag) were also analyzed to reveal background signals. Indicated are full-length Spt7–TAP (two exposures are shown) and CT-Spt7–TAP (C-terminal Spt7 fragment). (C) The cleavage efficiency of Spt7–TAP in the WT (lane 2 in B) and the *nup170*Δ mutant (lane 4 in B) were quantified. The ratio between the signal intensities of CT-Spt7–TAP (cleaved C-terminal fragment of Spt7) to full-length Spt7–TAP were measured in both strains. A relative Spt7–TAP cleavage efficiency was determined by normalizing to that of the WT cells and resulting ratios were plotted. Thus, the ratio for the WT is one. The individual observations are plotted as filled circles (n=4). There was a significant difference (as marked with the asterisk) for the ratio values between the WT and the *nup170*Δ strain as determined using a two-tailed paired t-test. (D) Spt20–TAP and associated proteins were purified from WT and *nup170*Δ cells producing Spt8-Myc. Total cell lysates (Input, 10%) and the purified protein complexes (IP) were analyzed by western blot using anti-Protein A and anti-Myc antibodies. Two exposures are shown of the anti-Myc antibody immunoblots. In all panels, the positions of mass markers are shown in kDa.

We propose that the increased cleavage of endogenous Spt7 and the NLS–tSpt7 reporter in the *nup170*Δ strain occurs as a consequence of increased diffusion of Pep4 into the nucleoplasm. To further test this idea, we examined whether loss of another Nup, Nup188, also previously shown to contribute to the NPC diffusion channel (Shulga et al., 2000), would similarly increase the cleavage of endogenous Spt7. For these experiments, Spt20–TAP was introduced into a *nup188*Δ mutant as well as two other mutant strains – one lacking Nup157 (a paralog of Nup170) and another lacking Pom152, two Nups not required for maintaining the passive diffusion barrier of the NPC (Shulga et al., 2000). Spt20–TAP was then purified from these mutant strains, and the levels of associated full-length Spt7 and its Pep4-dependent C-terminal truncation were compared. In the *nup157*Δ and *pom152*Δ mutants, the levels of Spt7 and its C-terminal

Journal of Cell Science (2020) 133, jcs237156. doi:10.1242/jcs.237156

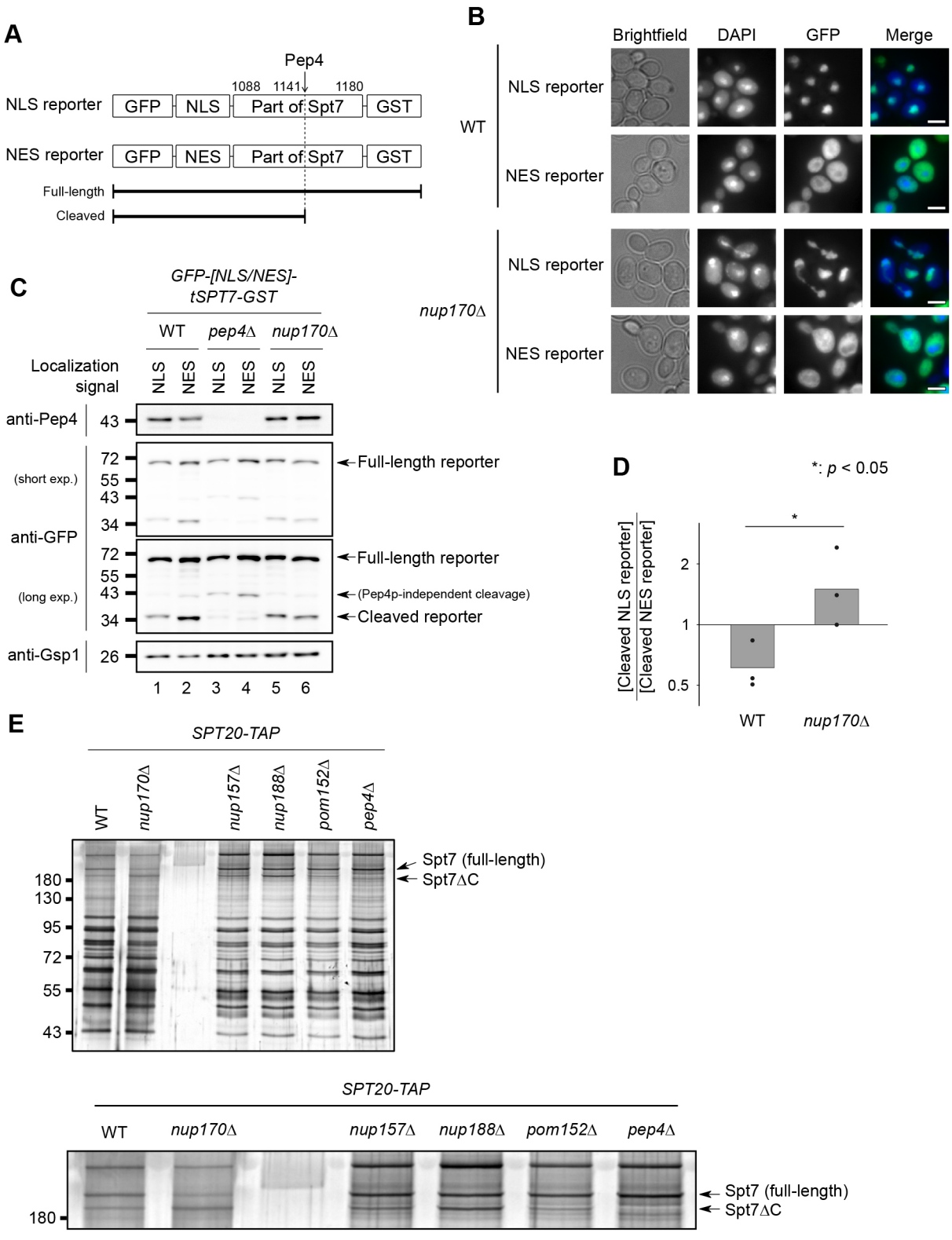

Fig. 4. See next page for legend.

truncation were similar to that detected in WT cells (Fig. 4E). However, like the *nup170*Δ mutant, the amount of the truncated Spt7 was increased in the *nup188*Δ mutant (Fig. 4E). These results support the conclusion that passive diffusion channels of the NPCs control accessibility of Pep4 to Spt7 and thus levels of the SLIK complex.

The passive diffusion properties of yeast NPCs are also altered by certain stress conditions induced by treatment of the cells with hydrogen peroxide or 1,6-hexanediol (Mason et al., 2005; Shulga and Goldfarb, 2003). Therefore, we tested the impact of treating cells with these compounds on the levels of SAGA and SLIK

Journal of Cell Science (2020) 133, jcs237156. doi:10.1242/jcs.237156

Fig. 4. The loss of Nup170 allows increased accessibility of Pep4 to the nucleoplasm. (A) Shown is a schematic diagram of the NLS and NES reporter proteins used for examining Pep4 activity in the cytoplasm and the nucleoplasm. The position of Pep4 cleavage site (following residue 1141) is indicated by an arrow. (B) WT and *nup170*Δ strains containing the reporter gene constructs were grown in YP raffinose medium supplemented with 2% galactose for 3 h to induce production of the NLS- and NES-reporter proteins depicted in A. The cells were fixed with 5% formaldehyde and examined using an epifluorescence microscope. Images showing the positions of cells (brightfield), nuclei (DAPI), reporter proteins (GFP) and merged images of DAPI and GFP (Merge) are shown. Scale bars: 5 µm. (C) WT, *pep4*Δ and *nup170*Δ strains containing the reporter gene constructs were induced to produce the nuclear GFP–*NLS*–tSpt7–GST (NLS) or cytoplasmic GFP–*NES*–tSpt7–GST (NES) reporter protein. Cell lysates were analyzed by western blotting using the indicated antibodies to detect Pep4, the full-length and cleaved NLS (lanes 1,3,5) and NES (lanes 2,4,6) reporter proteins (anti-GFP), and a loading control (Gsp1). Two exposures are shown of the anti-GFP immunoblots. In all panels, the positions of mass markers are shown in kDa. (D) The differences in efficiency of Pep4-dependent cleavage of the GFP–*NLS*–tSpt7–GST and GFP–*NES*–tSpt7–GST reporter proteins between the WT and *nup170*Δ strain were compared. The cleavage efficiencies of the reporter proteins were measured as the ratio between the signal intensities of cleaved reporters and the corresponding full-length proteins. A relative cleavage efficiency of the NLS reporter to that of the NES reporter was then calculated, and the resulting ratio was plotted on a $\log_2$ scale. The individual observations are plotted as filled circles (n=3), and the geometric mean values are plotted as bars. The ratio values show significant differences (asterisk) between WT and *nup170*Δ strains as determined using a two-tailed Student's *t*-test. (E) Spt20–TAP was purified from lysates of WT and the indicated mutant strains. Purified Spt20–TAP-containing complexes were analyzed by the SDS-PAGE and Silver staining. Two bands, the full-length Spt7 and the C-terminally truncated Spt7 (Spt7ΔC), are indicated by arrows. The image at the bottom shows a magnification of the Spt7 and Spt7ΔC containing-region of the top image. In all panels, the positions of mass markers are shown in kDa.

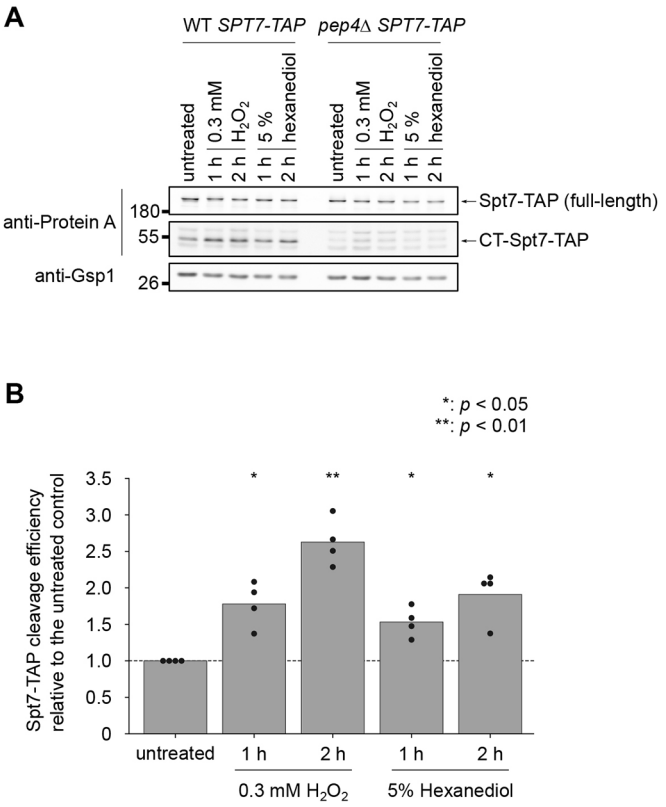

Fig. 5. Cell stress can induce increased Spt7 cleavage. (A) The WT and *pep4*Δ strains expressing *SPT7–TAP* were grown in YP glucose medium and harvested after treatment with or without hydrogen peroxide or 1,6-hexanediol at the indicated concentrations and times. Cell lysates were analyzed by western blotting using anti-Protein A (to detect Spt7–TAP and the cleaved CT-Spt7–TAP) and anti-Gsp1 antibodies (loading control). Note that the exposure time for Spt7–TAP is shorter than that for CT-Spt7-TAP (see similar example in Fig. 3B). (B) Spt7–TAP cleavage efficiencies under the various conditions relative to the untreated control in the WT background (WT *SPT7–TAP* in A) were determined as described in Fig. 3C. The individual observations are plotted as filled circles (n=4). Treatment conditions where the Spt7 cleavage was significantly increased compared to the untreated control, as determined by a two-tailed paired *t*-test, are indicated by asterisks.

complexes, again comparing levels of full-length and truncated Spt7 as a measure of the relative levels of these complexes. As shown in Fig. 5A,B, treatment of cells with hydrogen peroxide or 1,6-hexanediol led to Pep4-dependent increases in the cellular levels of the Spt7 truncation relative to full-length Spt7. Thus, similar to strains lacking Nup170 or Nup188, stress conditions previously shown to increase the size limits of the NPC passive diffusion channel also induce greater cleavage of Spt7 and an increase in the ratio of SLIK to SAGA complex.

Preventing Spt7 cleavage in the *nup170*Δ background partially reverses the reduced expression of the SAGA-dominated genes

On the basis of our analysis of the *nup170*Δ mutant, we predict that changes in cellular levels of the SAGA and SLIK complexes contribute to some of the observed alterations in transcription detected in this mutant. In order to investigate the effect of altering the SAGA–SLIK balance on the gene expression pattern, we prevented SLIK complex formation in the *nup170*Δ mutant by disrupting the *PEP4* gene, and we examined the effect of the *pep4*Δ mutation on the expression of ten SAGA-dominated genes previously shown to be downregulated in the *nup170*Δ mutant (Van De Vosse et al., 2013; see Fig. S1B). Our analysis confirmed significant mRNA decreases for eight of these genes in the *nup170*Δ mutant. Furthermore, as shown in Fig. 6 and Fig. S3, the reduced expression of several of these genes in the *nup170Δ* mutant was suppressed, at least partially, by the additional *pep4Δ* mutation, including significant increases in *CIS1, HIS4* and *ARG3* mRNA levels, while the mRNA levels of other genes, including *PDR5* and *PHO5*, were not altered by *PEP4* deletion. These results support the conclusion that at least a subset of the transcriptional reductions observed in the *nup170*Δ mutant are linked to Pep4-dependent cleavage of Spt7.

DISCUSSION

Transcriptome analysis of *nup170*Δ mutants revealed that Nup170 is required to repress the transcription of certain genes (Van De Vosse et al., 2013) while supporting the transcription of other genes (Van De Vosse et al., 2013; Fig. S1). These observations implicate Nup170 in distinct regulatory processes. In examining those genes that show reduced levels of transcripts in *nup170*Δ mutants, we observed that many are regulated by the SAGA transcriptional activator. Consistent with this, analyses of a subset of these genes in the *nup170*Δ mutant revealed reduced levels of bound preinitiation complex (PIC), including components of the SAGA complex, transcriptional activators and RNA Pol II. Concomitant with these changes are alterations in the relative cellular levels of the SAGA and SLIK complexes, with increased levels of the SLIK complex detected in the *nup170*Δ mutants. Nup170 does not appear to directly interact with the SAGA or SLIK complexes, but rather its role in mediating levels of these complexes is indirect and linked to changes in passive diffusion barrier of the NPC. These results lead

Journal of Cell Science (2020) 133, jcs237156. doi:10.1242/jcs.237156

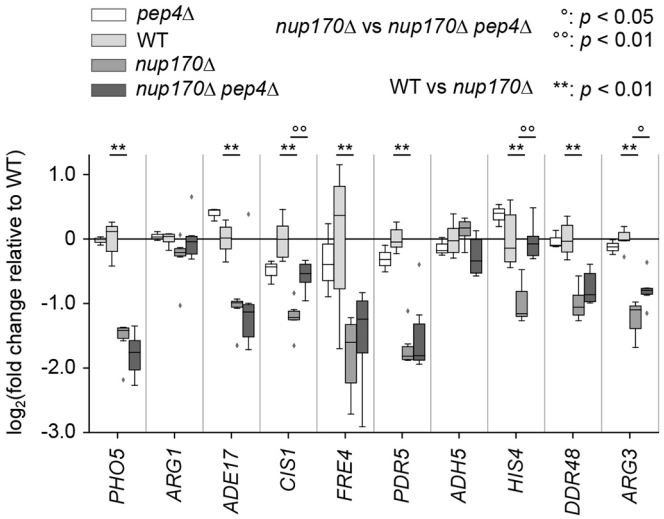

Fig. 6. Reduced expression of several genes in the *nup170*Δ mutant is Pep4-dependent. Total RNA was isolated from WT, *nup170*Δ, *pep4*Δ and *nup170*Δ *pep4*Δ mutant strains, and the mRNA levels of the indicated genes were examined by the qPCR. Levels of mRNA encoded by the indicated genes in each mutant were normalized to amounts in the WT strain. Fold changes in amounts detected in the mutants relative to WT cells were plotted on a $\log_2$ scale with a box-and-whisker plot (n=3 for *pep4*Δ, n=6 for WT, *nup170*Δ and *nup170*Δ *pep4*Δ). Boxes represent the first and third quartiles of the data points, and horizontal lines in the boxes represent the median. The whiskers extend over all the data points except outliers (defined as described in the Materials and Methods), plotted as diamonds. Significant differences in mRNA levels between the WT and the *nup170*Δ strain, as determined by a two-tailed paired *t*-test, are indicated by asterisks. For the genes exhibiting reduced mRNA levels in the *nup170*Δ strain, we further tested their mRNA levels between the *nup170*Δ and the *nup170*Δ *pep4*Δ strains. Significant differences (two-tailed paired *t*-test) in mRNA levels between the *nup170*Δ and the *nup170*Δ *pep4*Δ strains are indicated by open circles. All the observed data are plotted in Fig. S3.

us to propose that changes in passive diffusion rates through NPCs, as would occur during periods of altered cell physiology (e.g. stress) represents a mechanism for globally modulating nuclear functions, including transcriptional processes, such as those regulated by the SAGA and/or SLIK complexes.

Nups can influence gene expression by various mechanisms, including through their direct interactions with gene loci and the transcriptional machinery, or indirectly through their roles in regulating nuclear transport of transcriptional regulators. Some Nups are envisaged to contribute to multiple process, such as mammalian Nup98, which binds to and regulates the activity of nuclear transcription coactivators (Kasper et al., 1999) and RNA helicases (Capitanio et al., 2017, 2018), while also functioning in nuclear transport at NPCs (Powers et al., 1997; Oka et al., 2010). Transcriptional changes arising from mutations in such a multi-functional Nup are, therefore, likely to be a product of functional alterations in the various pathways that they contribute to and their cumulative impact on gene expression. Our analysis of the *nup170*Δ mutant suggests that this Nup can also influence transcription by multiple mechanisms. Previous studies have shown that Nup170 associates with subtelomeric chromatin and is required for the assembly of chromatin-associated silencing complexes containing Sir4 (Van De Vosse et al., 2013). In this instance, the loss of Nup170 reduced silencing of numerous subtelomeric genes leading to their increased expression. Notably, recent studies have shown that this function of Nup170 is likely performed by Nup170 that is present in a structure distinct from NPCs, termed the Snup complex, containing a subset of Nups and silencing factor Sir4 (Lapetina et al., 2017).

In addition to its role in promoting gene silencing, here, we report that Nup170 also supports active transcription of a subset of genes, most regulated by the SAGA complex (Fig. S1). Multiple observations lead us to conclude that Nup170 supports transcription indirectly. In support of this idea, we failed to detect physical interactions between Nup170 and SAGA complex components or members of the downregulated group of genes using IP or ChIP analysis (data not shown). Despite this, in cells lacking Nup170, the SAGA-regulated genes examined showed reduced levels of bound SAGA complex (Fig. 2B).

Consistent with the reduced levels of SAGA complex associated with genes normally regulated by this complex (Fig. 2), we also detected reduced cellular levels of SAGA complex relative to the related SLIK complex in the *nup170Δ* mutant (Fig. 3). A clue as to how Nup170 might influence the ratio of SAGA to SLIK complexes came from an examination of the mechanism of SLIK complex formation. Previous studies have shown that the SLIK complex arises from the cleavage of the SAGA complex component Spt7 by the vacuolar protease Pep4 (Spedale et al., 2010). The resulting truncated Spt7 fails to bind Spt8, the lack of which is a defining feature of the SLIK complex (Pray-Grant et al., 2002; Sterner et al., 2002). Of note, Spt8 is one of two SAGA components (along with Spt3) that interacts directly with the TATA-binding protein (TBP) (Han et al., 2014). As a consequence, the SLIK complex lacking Spt8 exhibits reduced binding to TBP (Sterner et al., 1999). This is consistent with our observation showing that the enrichment of Hfi1 (a common component of SAGA and SLIK) at the promoter regions of the SAGA-dependent genes examined was significantly reduced in the *nup170Δ* mutant (Fig. 2B).

We showed that the increased levels of the SLIK complex detected in the *nup170*Δ mutant were dependent on Pep4, leading us to conclude that loss of Nup170 was functioning to upregulate Pep4-mediated cleavage of Spt7. These data are consistent with previous literature identifying Pep4 as the protease responsible for cleavage of Spt7 and production of the SLIK complex (Spedale et al., 2010). Curiously, Pep4 is generally considered a luminal vacuolar protein. It contains a signal sequence that directs prepro-Pep4 to and across the ER membrane, and into the ER lumen. From there, Pep4 is transported to the vacuole lumen. It is there that a vacuolar protease activates Pep4 by removing its N-terminal propeptide (van den Hazel et al., 1996). Since SAGA and SLIK complexes reside and function in the nucleus (Pray-Grant et al., 2002; Spedale et al., 2010; also see Fig. S2A), it is difficult to envisage how a portion of SAGA complexes containing full-length Spt7 would enter vacuoles and then exit as SLIK complexes with cleaved Spt7. Piecemeal microautophagy of the nucleus (Roberts et al., 2003) or the macroautophagy (nucleophagy) (Mochida et al., 2015) could offer a mechanism for entry of the SAGA complex, or possibly Spt7 alone, into vacuoles. However, this mechanism seems unlikely as we have observed that cleavage of Spt7–TAP was not altered in mutants that inhibit microautophagy (*nvj1*Δ) and autophagy in general (*atg8*Δ) (Fig. S2B). Instead, for Pep4 to cleave nuclear Spt7, it is presumed that some portion of Pep4 must exit vacuoles and enter the cytoplasmic compartment. How this may occur is unknown; however, this is not an isolated phenomenon as other examples of vacuolar/lysosomal proteins functioning in the cytoplasmic/nuclear compartments have been reported, especially under stress conditions. For example, the endopolyphosphatase Ppn1 (Phm5) is processed to its enzymatically active, mature form in vacuoles but active Ppn1 is detected in the cytoplasm (Lichko et al., 2004; Shi

Journal of Cell Science (2020) 133, jcs237156. doi:10.1242/jcs.237156

and Kornberg, 2005; Reggiori and Pelham, 2001). In addition, various cytoplasmic tRNAs are cleaved by the vacuolar nuclease Rny1 (Thompson et al., 2008; Thompson and Parker, 2009). Nuclear activities of metazoan lysosomal enzymes have also been reported. The lysosomal protease cathepsin L is released from the lysosome and reaches the nucleus (Tholen et al., 2014) where it cleaves the CDP/Cux (CCAAT-displacement protein/cut homeobox) transcription factor to promote S phase progression (Goulet et al., 2004) and histone H3 during mouse embryonic stem cell differentiation (Duncan et al., 2008).

Our data also support the conclusion that Pep4 exits vacuoles, and enters the cytoplasm and the nucleus. Using reporter substrates containing the Pep4 cleavage site of Spt7 and either an NES or NLS, we were able to position the Pep4 substrate in the cytoplasm or the nucleus and assay for their cleavage. Both substrates exhibited Pep4-dependent cleavage in WT and *nup170*Δ cells (Fig. 4). These results support the conclusion that Pep4 can enter the nucleus where it would have access to endogenous Spt7. Importantly, in the *nup170*Δ mutant, cleavage of the nuclear NLS-containing reporter was increased, while cleavage of the cytoplasmic NES-containing reporter appeared reduced, leading to an increase in the ratio of the NLS-reporter:NES-reporter cleavage products (Fig. 4D). These data are consistent with the higher levels of the Spt7 truncation detected in the *nup170*Δ mutant (Fig. 3A–C), and they suggest this phenotype arises from increased levels of Pep4 in the nucleus in the *nup170*Δ mutant. Of note, attaching a tag (GFP and HA) to Pep4 for the purpose of examining its localization was not useful, as these tagged forms of Pep4 appeared to be unstable and their cellular levels were severely reduced relative to untagged Pep4. Consistent with this observation, cells producing Pep4–GFP showed reduced cleavage of Spt7 (data not shown).

We were posed with the question of how Pep4, once released from vacuoles, would enter the nucleoplasm, and why entry is more efficient in *nup170*Δ cells. We conclude that Pep4 entry into the nucleus is unlikely to be mediated by NTFs. First, Pep4 lacks any detectable NLSs within its primary sequence that would facilitate nuclear import. Second, the increase in nuclear Pep4 activity detected in the *nup170*Δ mutant was also unlikely to be explained by increased NTF-mediated nuclear import, as transport changes of this type have not been observed in the *nup170*Δ mutant (Shulga et al., 2000). Instead, an alternative explanation is that movement of Pep4 across the NE and into the nucleus is controlled by the passive diffusion barrier of NPCs. Consistent with this idea, previous studies have shown that the ‘sieving limit’ for the NPC diffusion channel is greater in cells lacking Nup170 (Shulga et al., 2000; Timney et al., 2016). Shulga et al. also showed an increase in the size of the NPC diffusion channel in cells lacking Nup188, a binding partner of Nup170 within the inner ring complex of the NPC. By contrast, the loss of two other Nup170-binding partners, Nup157 and Pom152, does not alter the diffuse rates through NPCs (Shulga et al., 2000). Consistent with the roles of these various Nups in passive diffusion, the levels of the Spt7 truncations (i.e. Pep4 cleavage) were increased in the *nup170*Δ and *nup188*Δ mutants, whereas mutants that did not affect diffusion (*nup157*Δ and *pom152*Δ) contained WT levels of the Spt7 truncation (Fig. 4E). Moreover, in comparing the *nup170*Δ and *nup188*Δ mutants, we observed that the higher sieving limits reported for NPCs lacking Nup170 versus those lacking Nup188 (Shulga et al., 2000) directly correlated with higher levels of truncated Spt7 in the *nup170*Δ mutant as compared to in the *nup188*Δ mutant (Fig. 4E). The more moderate effects of the *nup188*Δ mutant are also reflected in the reduced impact of this mutant on the expression of the SAGA genes analyzed in Fig. 6, where genes including *HIS4*, which exhibit Pep4-dependent reduction in the *nup170*Δ mutant, showed little or no change in expression in the *nup188*Δ mutant (Fig. S4).

Cumulatively, the results presented in this article suggest that the properties of the passive diffusion channel of the NPC can function to mediate levels of transcriptional complexes in the nucleoplasm. Specifically, our study revealed that the relative abundance of the SAGA and SLIK complexes are influenced by Pep4, and the passive diffusion properties of the NPC. We envisage that there are likely other examples of factors controlling nuclear functions whose entry into the nucleus are mediated by the NPC passive diffusion barrier rather than facilitated NTF-mediated transport. Moreover, this may include a broader spectrum of cytoplasmic molecules than previously considered. This is emphasized by recent work from Timney et al. (2016) suggesting that the NPC does not impose a strict passive diffusion limit but rather it functions as a soft barrier that gradually restricts the movement of molecules as they increase in mass. These observations suggest that molecules of greater mass than previously anticipated can passively diffuse across the NE, albeit with decreased rates as their size increases. Consistent with this idea, many proteins and protein complexes of up to ∼100 kDa (and lacking nuclear transport signals) appear to partition equally between the cytoplasm and the nucleoplasm (Wühr et al., 2015).

Our observations that specific transcriptional events, such as those controlled by the SAGA and SLIK complexes, are linked to the state of the passive diffusion barrier suggest that conditions that alter its properties, such as stress, represent a potential control point for regulating transcription and other nuclear functions. In support of such a mechanism, previous studies have shown that stressing yeast cells through treatment with hydrogen peroxide induces an increase in the size of the NPC passive diffusion channel (Mason et al., 2005), and, as shown in Fig. 5, an increase in levels of the Spt7 truncation and the SLIK complex. Of note, cellular responses to other stress conditions have also been linked to the activity of the SLIK complex (Spedale et al., 2010). For example, mutant cells in which the SLIK complex predominates are more resistant to the growth inhibitory effects of rapamycin treatment than WT cells, while cells in which SAGA is predominant are more sensitive to rapamycin than WT (Spedale et al., 2010).

Our observations that transcriptional changes in the *nup170*Δ mutant arise from the loss of several distinct functions of this Nup suggests that one must generally consider the multifunctional potential of any Nup, including a role in the passive diffusion barrier, when assessing its roles in nuclear functions, such as transcriptional regulation. With this in mind, it will be of future interest to assess the similarities and differences in the transcriptome profiles of various *nup* mutants that alter the passive diffusion barrier. This may provide clues as to the broader effects of altering the passive diffusion barrier on transcription, and whether specific Nups, through their signature impacts on passive diffusion, may influence specific transcriptional events. We speculate that physiological or environmental changes that alter the function of Nups forming the passive diffusion barrier, either through their modification or degradation, could represent a mechanism for transiently regulating transcription, for example during periods of stress (as discussed above) or in response changes in growth, cell shape or during developmental stages when the passive diffusion barrier also changes (Feldherr and Akin, 1990; Jiang and Schindler, 1988; García-González et al., 2018). In addition, continuous and irreversible changes in the permeability of NPCs have been proposed to occur in post-mitotic metazoan cells as they age (D’Angelo et al., 2009). This has been suggested to arise as a

consequence of accumulated damage to long-lived Nups, including Nup155, the mammalian counterpart of Nup170 (D'Angelo et al., 2009; Savas et al., 2012). The consequences of these age-related changes in the passive diffusion barrier of the NPC remain to be determined, but it seems reasonable to speculate that many nuclear functions are impacted, including transcription. Similarly, it is important to consider whether disease states linked to mutations in the human counterparts of several yeast Nups, such as Nup170, Nup188 and Nup116 (Zhang et al., 2008; Simon and Rout, 2014; Haskell et al., 2017; Beck and Hurt, 2017), occur as a consequence of constitutive defects in the passive diffusion barrier.

MATERIALS AND METHODS

Yeast strains and cultures

Yeast strains used in this study are shown in Table S4. All strains were grown in YP medium (1% yeast extract, 2% peptone) plus an appropriate carbon source (2% glucose or 2% raffinose) at 30°C. For the gene induction under control of *GAL1* promoter, galactose (from a 20% stock solution) was added directly into the culture medium to a final concentration of 2%. For stress treatment with hydrogen peroxide and 1,6-hexanediol, the chemicals from stock solutions (100 mM hydrogen peroxide and 50% 1,6-hexanediol in water) were directly added to the medium.

Western blotting

For analyzing the whole-cell lysate of yeast in normal growing conditions, cells were grown in the YP glucose medium at 30°C to an optical density at 600 nm (OD_{600}) of ∼1.0. For preparing yeast cells after galactose induction, cells were grown in the YP raffinose medium to OD_{600} of ∼0.5, followed by incubation with an additional 2% galactose for 3 h. Cells were harvested from 1 ml of culture with a cell density of OD_{600} ∼1.0 and resuspended in 100 µl of SDS-PAGE sample buffer, followed by brief sonication and heat denaturation at 65°C for 10 min. The protein samples were separated by SDS-PAGE and transferred on the nitrocellulose membranes. Proteins were detected by western blotting using anti-Protein A from rabbit (for detecting TAP fusion proteins; 1:10,000, P3775; Sigma), anti-Gsp1 from rabbit (1:10,000; Makhnevych et al., 2003), anti-Pep4 from rabbit (1:5000; a gift from Dr Gary Eitzen, University of Alberta, Edmonton, Canada), anti-Myc from mouse (1:10,000; 9E10; 11667149001; Roche) and anti-HA from mouse (1:10,000; 12CA5; 11583816001; Roche) and anti-GFP from mouse (1:10,000; clones 7.1 and 13.1; 11814460001; Roche), and HRP-conjugated anti-rabbit IgG and anti-mouse IgG (Bio-Rad) secondary antibodies. The protein signals were visualized using ECL western blotting detection reagent (GE Healthcare), and scanned using an ImageQuant LAS 4000 (GE Healthcare) imaging system.

mRNA extraction and qPCR

Total RNA from yeast was extracted by the hot phenol method (Van De Vosse et al., 2013). Yeast culture (10 ml) was grown to an OD_{600} of 0.8–1.0. Cells derived from 5 ml of culture with a cell density of OD_{600} ∼1.0 were collected and resuspended in 0.5 ml TES (10 mM Tris-HCl pH 7.5, 1 mM EDTA and 100 mM NaCl). The suspension was well mixed with 0.5 ml water-saturated phenol through vortexing. Then the sample was incubated for 1 h at 65°C in order to extract RNA from the cells. After centrifugation (20,000 ***g*** for 5 min), the water layer containing RNA was further purified by mixing with phenol:chloroform:isoamyl alcohol (25:24:1). The RNA was precipitated with ethanol, dried and dissolved in DEPC water. Total RNA (2 µg) was subjected to reverse transcription using the Superscript II kit (Life Technologies). The relative gene abundance in the cDNA sample was examined by qPCR on a MX3000 (Agilent) machine using PerfeCTa SYBR Green PCR mix (Quanta Bioscience). Primers for the qPCR reaction are given in Table S5. The change in the mRNA level of the genes among various mutants were evaluated by the $\Delta\Delta C_T$ method (Livak and Schmittgen, 2001). The C_T value for each gene target was normalized against the internal control (*ACT1* and *TUB1*) to give the ΔC_T value. The $\Delta\Delta C_T$ was calculated as a difference in ΔC_T values between the mutant and the WT strain. The change in the mRNA level of the genes among the mutant was given as $2^{-\Delta\Delta CT}$, based on the assumption that amplification efficiency of the PCR reaction is 100%.

Chromatin immunoprecipitation

ChIP experiments were performed as described previously (Hecht and Grunstein, 1999; Van De Vosse et al., 2013). A total of 50 ml of culture at an OD_{600} of 0.8–1.0 was subjected to crosslinking with 4% formaldehyde for 20 min at room temperature. The crosslinking reaction was quenched by incubation with 125 mM glycine for 5 min. Cells were resuspended in lysis buffer (50 mM HEPES-KOH, pH 7.5, 140 mM NaCl, 1 mM EDTA, 1% Triton X-100 and 0.1% sodium deoxycholate) and disrupted by vortexing in the presence of glass beads, and the chromatin DNA was sheared by sonication (Branson Sonifer 250) to an average fragment size of 300–500 bp. The lysate was incubated with 3 µg of antibodies [anti-V5 (SV5-Pk1; ab27671; Abcam), anti-HA (12CA5; 11583816001; Roche), anti-Rpb3p (1Y26 (1Y27); ab81859; Abcam) or anti-Histone H3 (ab46765; Abcam)] and a 50 µl suspension (1.5 mg of beads) of Protein G-conjugated Dynabeads (Life Technologies) for 2 h at 4°C. Chromatin regions captured by Dynabeads were collected with magnetic stands. After washing, crosslinks were reversed by incubation at 65°C overnight.

The enrichment of chromatin regions was examined by qPCR on MX3000 (Agilent) using PerfeCTa SYBR Green PCR mix (Quanta Biosciences). Oligonucleotides used for the qPCR are summarized in Table S5. Relative enrichment of the gene loci immunoprecipitated with the protein of interest was evaluated by the $\Delta\Delta C_T$ method (Livak and Schmittgen, 2001). The C_T values for the amplicon from the IP sample were firstly normalized against the corresponding input to give the ΔC_T values. The $\Delta\Delta C_T$ value was calculated as a difference in ΔC_T values between the gene locus of interest and the non-transcribed control (ChrV-1, ChrV-2 and ChrII-1). These non-transcribed controls are located in the middle of a >1 kbp region without any observed transcription [open reading frames (ORFs), stable uncharacterized transcripts, cryptic unstable transcripts or other RNA polymerase-dependent transcription] (Xu et al., 2009). The relative enrichment of the specific genomic loci over background was given as $2^{-\Delta\Delta CT}$, based on the assumption that amplification efficiency of the PCR reaction is 100%.

Immunoisolation of the SAGA and SLIK complexes, and mass spectrometry analysis

Cells derived from a 1 liter culture (OD_{600} of 1.0) of a strain expressing *SPT20–TAP* were collected and flash frozen with liquid nitrogen. Cell samples were subjected to cryogrinding (Retsch PM100) to produce frozen lysate powder (Oeffinger et al., 2007). Lysate powder (1 g) was resuspended in the IP buffer (20 mM HEPES-KOH pH 7.5, 110 mM potassium acetate, 100 mM NaCl, 2 mM $MgCl_2$, 0.1% Tween 20, 5% glycerol) plus cOmplete protease inhibitor cocktail without EDTA (Roche). The suspension was clarified by a series of consecutive centrifugations (500 ***g*** for 10 min, 20,000 ***g*** for 20 min and 100,000 ***g*** for 1 h) and the supernatant was collected. The cleared lysate was incubated with 3 mg IgG-conjugated Dynabeads for 1 h at 4°C. The beads were collected using a magnetic stand and washed five times with the IP buffer (without protease inhibitor cocktail). The protein complexes bound to the beads were released by a treatment with TEV protease (kindly provided by Dr Ben Montpetit, University of California Davis) for 1 h at room temperature. Proteins released from the beads were precipitated with 10% trichloroacetic acid (TCA) and resuspended in SDS-PAGE sample buffer.

Isolated proteins were separated on the SDS-PAGE gels and visualized through Coomassie Brilliant Blue (CBB), silver staining or western blotting. For mass spectrometry analysis, the protein samples in the CBB-stained gels were excised and submitted to the Alberta Proteomics and Mass Spectrometry Facility (Department of Biochemistry, University of Alberta) for identification. The data were analyzed with the software Proteome Discoverer (Thermo Fisher Scientific).

Microscopy

Cells producing the indicated GFP fusion proteins were grown to an OD_{600} of ∼1.0, and fixed with 5% formaldehyde in 100 mM potassium phosphate,

pH 6.5 for 10 min. The fixed cells were washed with PBS twice and resuspended in a mounting medium (Dapi Fluoromount-G; Southern Biotech). The samples were put on microscope slides, and the images were observed on an AxioObserver.Z1 microscope (Zeiss) equipped with an UPlanS-Apochromat 100×/1.40 NA oil objective lens (Zeiss) and an AxioCam MRm digital camera with a charge-coupled device (Zeiss). Image manipulations (cropping and normalization) were performed with the software ImageJ (NIH).

Statistical analysis

Pairwise comparisons were made using a two-tailed unpaired *t*-test (Student's *t*-test) or a two-tailed paired *t*-test as indicated in each figure. The numbers of independent observations (*n*) are specified. The data are plotted using Microsoft Excel or the plotting library Seaborn (https://seaborn.pydata.org/). Outliers in Fig. 6 are defined by Seaborn as the data points with values less than Q1−1.5×IQR or larger than Q3+1.5×IQR, where Q1 is the first quartile, Q3 is the third quartile, and the IQR=Q3−Q1.

Acknowledgements

We thank Dr Ben Montpetit (University of California, Davis) and Dr Gary Eitzen (University of Alberta) for providing the indicated reagents. We also thank B. Montpetit for critical reading of the manuscript.

Competing interests

The authors declare no competing or financial interests.

Author contributions

Conceptualization: T.M., R.W.W.; Methodology: T.M., R.W.W.; Validation: T.M.; Formal analysis: T.M., R.W.W.; Investigation: T.M.; Writing - original draft: T.M., R.W.W.; Writing - review & editing: T.M., R.W.W.; Visualization: T.M., R.W.W.; Supervision: R.W.W.; Project administration: R.W.W.; Funding acquisition: R.W.W.

Funding

Funding for this work is supported by Canadian Institutes of Health Research (MOP 106502).

Supplementary information

Supplementary information available online at http://jcs.biologists.org/lookup/doi/10.1242/jcs.237156.supplemental

Peer review history

The peer review history is available online at https://jcs.biologists.org/lookup/doi/10.1242/jcs.237156.reviewer-comments.pdf

References

Aitchison, J. D. and Rout, M. P. (2012). The yeast nuclear pore complex and transport through it. *Genetics* **190**, 855-883. doi:10.1534/genetics.111.127803

Barbaric, S., Reinke, H. and Hörz, W. (2003). Multiple mechanistically distinct functions of SAGA at the PHO5 promoter. *Mol. Cell. Biol.* **23**, 3468-3476. doi:10.1128/MCB.23.10.3468-3476.2003

Beck, M. and Hurt, E. (2017). The nuclear pore complex: understanding its function through structural insight. *Nat. Rev. Mol. Cell Biol.* **18**, 73-89. doi:10.1038/nrm.2016.147

Capitanio, J. S., Montpetit, B. and Wozniak, R. W. (2017). Human nup98 regulates the localization and activity of DExH/D-box helicase DHX9. *eLife* **6**, e18825. doi:10.7554/eLife.18825

Capitanio, J. S., Montpetit, B. and Wozniak, R. W. (2018). Nucleoplasmic Nup98 controls gene expression by regulating a DExH/D-box protein. *Nucleus* **9**, 1-8. doi:10.1080/19491034.2017.1364826

D'Angelo, M. A., Raices, M., Panowski, S. H. and Hetzer, M. W. (2009). Age-dependent deterioration of nuclear pore complexes causes a loss of nuclear integrity in postmitotic cells. *Cell* **136**, 284-295. doi:10.1016/j.cell.2008.11.037

Duncan, E. M., Muratore-Schroeder, T. L., Cook, R. G., Garcia, B. A., Shabanowitz, J., Hunt, D. F. and Allis, C. D. (2008). Cathepsin L proteolytically processes histone H3 during mouse embryonic stem cell differentiation. *Cell* **135**, 284-294. doi:10.1016/j.cell.2008.09.055

Feldherr, C. M. and Akin, D. (1990). The permeability of the nuclear envelope in dividing and nondividing cell cultures. *J. Cell Biol.* **111**, 1-8. doi:10.1083/jcb.111.1.1

García-González, A., Jacchetti, E., Marotta, R., Tunesi, M., Rodríguez Matas, J. F. and Raimondi, M. T. (2018). The effect of cell morphology on the permeability of the nuclear envelope to diffusive factors. *Front. Physiol.* **9**, 1-15. doi:10.3389/fphys.2018.00925

Goulet, B., Baruch, A., Moon, N.-S., Poirier, M., Sansregret, L. L., Erickson, A., Bogyo, M. and Nepveu, A. (2004). A cathepsin L isoform that is devoid of a signal peptide localizes to the nucleus in S phase and processes the CDP/Cux transcription factor. *Mol. Cell* **14**, 207-219. doi:10.1016/S1097-2765(04)00209-6

Han, Y., Luo, J., Ranish, J. and Hahn, S. (2014). Architecture of the Saccharomyces cerevisiae SAGA transcription coactivator complex. *EMBO J.* **33**, 2534-2546. doi:10.15252/embj.201488638

Hartley, P. D. and Madhani, H. D. (2009). Mechanisms that specify promoter nucleosome location and identity. *Cell* **137**, 445-458. doi:10.1016/j.cell.2009.02.043

Haskell, G. T., Jensen, B. C., Samsa, L. A., Marchuk, D., Huang, W., Skrzynia, C., Tilley, C., Seifert, B. A., Rivera-Muñoz, E. A., Koller, B. et al. (2017). Whole exome sequencing identifies truncating variants in nuclear envelope genes in patients with cardiovascular disease. *Circ. Cardiovasc. Genet.* **10**, 1-11. doi:10.1161/CIRCGENETICS.116.001443

Hecht, A. and Grunstein, M. (1999). Mapping DNA interaction sites of chromosomal proteins using immunoprecipitation and polymerase chain reaction. *Methods Enzymol.* **304**, 399-414. doi:10.1016/S0076-6879(99)04024-0

Huisinga, K. L. and Pugh, B. F. (2004). A genome-wide housekeeping role for TFIID and a highly regulated stress-related role for SAGA in Saccharomyces cerevisiae. *Mol. Cell* **13**, 573-585. doi:10.1016/S1097-2765(04)00087-5

Hülsmann, B. B., Labokha, A. A. and Görlich, D. (2012). The permeability of reconstituted nuclear pores provides direct evidence for the selective phase model. *Cell* **150**, 738-751. doi:10.1016/j.cell.2012.07.019

Ibarra, A. and Hetzer, M. W. (2015). Nuclear pore proteins and the control of genome functions. *Genes Dev.* **29**, 337-349. doi:10.1101/gad.256495.114

Jiang, L. W. and Schindler, M. (1988). Nuclear transport in 3T3 fibroblasts: effects of growth factors, transformation, and cell shape. *J. Cell Biol.* **106**, 13-19. doi:10.1083/jcb.106.1.13

Kasper, L. H., Brindle, P. K., Schnabel, C. A., Pritchard, C. E. J., Cleary, M. L. and van Deursen, J. M. A. (1999). CREB binding protein interacts with nucleoporin-specific FG repeats that activate transcription and mediate NUP98-HOXA9 oncogenicity. *Mol. Cell. Biol.* **19**, 764-776. doi:10.1128/MCB.19.1.764

Lapetina, D. L., Ptak, C., Roesner, U. K. and Wozniak, R. W. (2017). Yeast silencing factor Sir4 and a subset of nucleoporins form a complex distinct from nuclear pore complexes. *J. Cell Biol.* **216**, 3145-3159. doi:10.1083/jcb.201609049

Lichko, L., Kulakovskaya, T. and Kulaev, I. (2004). Inactivation of endopolyphosphatase gene PPN1 results in inhibition of expression of exopolyphosphatase PPX1 and high-molecular-mass exopolyphosphatase not encoded by PPX1 in Saccharomyces cerevisiae. *Biochim. Biophys. Acta Gen. Subj.* **1674**, 98-102. doi:10.1016/j.bbagen.2004.06.004

Livak, K. J. and Schmittgen, T. D. (2001). Analysis of relative gene expression data using real-time quantitative PCR and the 2(−Delta Delta C(T)) Method. *Methods* **25**, 402-408. doi:10.1006/meth.2001.1262

López-Otín, C., Blasco, M. A., Partridge, L., Serrano, M. and Kroemer, G. (2013). The hallmarks of aging. *Cell* **153**, 1194. doi:10.1016/j.cell.2013.05.039

Lowe, A. R., Siegel, J. J., Kalab, P., Siu, M., Weis, K. and Liphardt, J. T. (2010). Selectivity mechanism of the nuclear pore complex characterized by single cargo tracking. *Nature* **467**, 600-603. doi:10.1038/nature09285

Makhnevych, T., Lusk, C. P., Anderson, A. M., Aitchison, J. D. and Wozniak, R. W. (2003). Cell cycle regulated transport controlled by alterations in the nuclear pore complex. *Cell* **115**, 813-823. doi:10.1016/S0092-8674(03)00986-3

Mason, D. A., Shulga, N., Undavai, S., Ferrando-May, E., Rexach, M. F. and Goldfarb, D. S. (2005). Increased nuclear envelope permeability and Pep4p-dependent degradation of nucleoporins during hydrogen peroxide-induced cell death. *FEMS Yeast Res.* **5**, 1237-1251. doi:10.1016/j.femsyr.2005.07.008

Mischerikow, N., Spedale, G., Altelaar, A. F. M., Timmers, H. T. M., Pijnappel, W. W. M. P. and Heck, A. J. R. (2009). In-depth profiling of post-translational modifications on the related transcription factor complexes TFIID and SAGA. *J. Proteome Res.* **8**, 5020-5030. doi:10.1021/pr900449e

Mochida, K., Oikawa, Y., Kimura, Y., Kirisako, H., Hirano, H., Ohsumi, Y. and Nakatogawa, H. (2015). Receptor-mediated selective autophagy degrades the endoplasmic reticulum and the nucleus. *Nature* **522**, 359-362. doi:10.1038/nature14506

Oeffinger, M., Wei, K. E., Rogers, R., DeGrasse, J. A., Chait, B. T., Aitchison, J. D. and Rout, M. P. (2007). Comprehensive analysis of diverse ribonucleoprotein complexes. *Nat. Methods* **4**, 951-956. doi:10.1038/nmeth1101

Oka, M., Asally, M., Yasuda, Y., Ogawa, Y., Tachibana, T. and Yoneda, Y. (2010). The mobile FG Nucleoporin Nup98 is a cofactor for Crm1-dependent protein export. *Mol. Biol. Cell* **21**, 1885-1896. doi:10.1091/mbc.e09-12-1041

Paine, P. L. (1975). Nucleocytoplasmic movement of fluorescent tracers microinjected into living salivary gland cells. *J. Cell Biol.* **66**, 652-657. doi:10.1083/jcb.66.3.652

Paine, P. L. and Feldherr, C. M. (1972). Nucleocytoplasmic exchange of macromolecules. *Exp. Cell Res.* **74**, 81-98. doi:10.1016/0014-4827(72)90483-1

Peters, R. (1983). Nuclear envelope permeability measured by fluorescence microphotolysis of single liver cell nuclei. *J. Biol. Chem.* **258**, 11427-11429.

Popken, P., Ghavami, A., Onck, P. R., Poolman, B. and Veenhoff, L. M. (2015). Size-dependent leak of soluble and membrane proteins through the yeast nuclear pore complex. *Mol. Biol. Cell* **26**, 1386-1394. doi:10.1091/mbc.E14-07-1175

Powers, M. A., Forbes, D. J., Dahlberg, J. E. and Lund, E. (1997). The vertebrate GLFG nucleoporin, Nup98, is an essential component of multiple RNA export pathways. *J. Cell Biol.* **136**, 241-250. doi:10.1083/jcb.136.2.241

Pray-Grant, M. G., Schieltz, D., McMahon, S. J., Wood, J. M., Kennedy, E. L., Cook, R. G., Workman, J. L., Yates, J. R., III and Grant, P. A. (2002). The novel SLIK histone acetyltransferase complex functions in the yeast retrograde response pathway. *Mol. Cell. Biol.* **22**, 8774-8786. doi:10.1128/MCB.22.24.8774-8786.2002

Ptak, C. and Wozniak, R. W. (2016). Nucleoporins and chromatin metabolism. *Curr. Opin. Cell Biol.* **40**, 153-160. doi:10.1016/j.ceb.2016.03.024

Ptak, C., Aitchison, J. D. and Wozniak, R. W. (2014). The multifunctional nuclear pore complex: a platform for controlling gene expression. *Curr. Opin. Cell Biol.* **28**, 46-53. doi:10.1016/j.ceb.2014.02.001

Reggiori, F. and Pelham, H. R. B. (2001). Sorting of proteins into multivesicular bodies: ubiquitin-dependent and -independent targeting. *EMBO J.* **20**, 5176-5186. doi:10.1093/emboj/20.18.5176

Roberts, P., Moshitch-Moshkovitz, S., Kvam, E., O'Toole, E., Winey, M. and Goldfarb, D. S. (2003). Piecemeal Microautophagy of Nucleus in Saccharomyces cerevisiae. *Mol. Biol. Cell.* **14**, 129-141. doi:10.1091/mbc.e02-08-0483

Rout, M. P., Aitchison, J. D., Magnasco, M. O. and Chait, B. T. (2003). Virtual gating and nuclear transport: the hole picture. *Trends Cell Biol.* **13**, 622-628. doi:10.1016/j.tcb.2003.10.007

Savas, J. N., Toyama, B. H., Xu, T., Yates, J. R. and Hetzer, M. W. (2012). Extremely long-lived nuclear pore proteins in the rat brain. *Science.* **335**, 942. doi:10.1126/science.1217421

Shi, X. and Kornberg, A. (2005). Endopolyphosphatase in Saccharomyces cerevisiae undergoes post-translational activations to produce short-chain polyphosphates. *FEBS Lett.* **579**, 2014-2018. doi:10.1016/j.febslet.2005.02.032

Shulga, N. and Goldfarb, D. S. (2003). Binding dynamics of structural nucleoporins govern nuclear pore complex permeability and may mediate channel gating. *Mol. Cell. Biol.* **23**, 534-542. doi:10.1128/MCB.23.2.534-542.2003

Shulga, N., Mosammaparast, N., Wozniak, R. and Goldfarb, D. S. (2000). Yeast nucleoporins involved in passive nuclear envelope permeability. *J. Cell Biol.* **149**, 1027-1038. doi:10.1083/jcb.149.5.1027

Simon, D. N. and Rout, M. P. (2014). Cancer and the Nuclear pore complex. *Adv. Exp. Med. Biol.* **773**, 285-307. doi:10.1007/978-1-4899-8032-8_13

Spedale, G., Mischerikow, N., Heck, A. J. R., Timmers, H. T. M. and Pijnappel, W. W. M. P. (2010). Identification of Pep4p as the Protease Responsible for Formation of the SAGA-related SLIK Protein Complex. *J. Biol. Chem.* **285**, 22793-22799. doi:10.1074/jbc.M110.108787

Sterner, D. E., Grant, P. A., Roberts, S. M., Duggan, L. J., Belotserkovskaya, R., Pacella, L. A., Winston, F., Workman, J. L. and Berger, S. L. (1999). Functional Organization of the Yeast SAGA complex: distinct components involved in structural integrity, nucleosome acetylation, and TATA-binding protein interaction. *Mol. Cell. Biol.* **19**, 86-98. doi:10.1128/MCB.19.1.86

Sterner, D. E., Belotserkovskaya, R. and Berger, S. L. (2002). SALSA, a variant of yeast SAGA, contains truncated Spt7, which correlates with activated transcription. *Proc. Natl. Acad. Sci. USA* **99**, 11622-11627. doi:10.1073/pnas.182021199

Therizols, P., Fairhead, C., Cabal, G. G., Genovesio, A., Dujon, B., Fabre, E., Olivo-Marin, J.-C., Dujon, B. and Fabre, E. (2006). Telomere tethering at the nuclear periphery is essential for efficient DNA double strand break repair in subtelomeric region. *J. Cell Biol.* **172**, 189-199. doi:10.1083/jcb.200505159

Tholen, M., Hillebrand, L. E., Tholen, S., Sedelmeier, O., Arnold, S. J. and Reinheckel, T. (2014). Out-of-frame start codons prevent translation of truncated nucleo-cytosolic cathepsin L in vivo. *Nat. Commun.* **5**, 4931. doi:10.1038/ncomms5931

Thompson, D. M. and Parker, R. (2009). The RNase Rny1p cleaves tRNAs and promotes cell death during oxidative stress in Saccharomyces cerevisiae. *J. Cell Biol.* **185**, 43-50. doi:10.1083/jcb.200811119

Thompson, D. M., Lu, C., Green, P. J. and Parker, R. (2008). tRNA cleavage is a conserved response to oxidative stress in eukaryotes. *RNA.* **14**, 2095-2103. doi:10.1261/rna.1232808

Timney, B. L., Raveh, B., Mironska, R., Trivedi, J. M., Kim, S. J., Russel, D., Wente, S. R., Sali, A. and Rout, M. P. (2016). Simple rules for passive diffusion through the nuclear pore complex. *J. Cell Biol.* **215**, 57-76. doi:10.1083/jcb.201601004

Van De Vosse, D. W., Wan, Y., Lapetina, D. L., Chen, W.-M., Chiang, J.-H., Aitchison, J. D. and Wozniak, R. W. (2013). A role for the nucleoporin Nup170p in chromatin structure and gene silencing. *Cell.* **152**, 969-983. doi:10.1016/j.cell.2013.01.049

van den Hazel, H. B., Kielland-Brandt, M. C. and Winther, J. R. (1996). Review: biosynthesis and function of yeast vacuolar proteases. *Yeast.* **12**, 1-16. doi:10.1002/(SICI)1097-0061(199601)12:1<1::AID-YEA902>3.0.CO;2-N

Wang, R. and Brattain, M. G. (2007). The maximal size of protein to diffuse through the nuclear pore is larger than 60 kDa. *FEBS Lett.* **581**, 3164-3170. doi:10.1016/j.febslet.2007.05.082

Wente, S. R. and Rout, M. P. (2010). The nuclear pore complex and nuclear transport. *Cold Spring Harb. Perspect. Biol.* **2**, a000562. doi:10.1101/cshperspect.a000562

Wühr, M., Güttler, T., Peshkin, L., McAlister, G. C., Sonnett, M., Ishihara, K., Groen, A. C., Presler, M., Erickson, B. K., Mitchison, T. J. et al. (2015). The nuclear proteome of a vertebrate. *Curr. Biol.* **25**, 2663-2671. doi:10.1016/j.cub.2015.08.047

Xu, Z., Wei, W., Gagneur, J., Perocchi, F., Clauder-Münster, S., Camblong, J., Guffanti, E., Stutz, F., Huber, W. and Steinmetz, L. M. (2009). Bidirectional promoters generate pervasive transcription in yeast. *Nature* **457**, 1033-1037. doi:10.1038/nature07728

Zhang, X., Chen, S., Yoo, S., Chakrabarti, S., Zhang, T., Ke, T., Oberti, C., Yong, S. L., Fang, F., Li, L. et al. (2008). Mutation in nuclear pore component NUP155 leads to atrial fibrillation and early sudden cardiac death. *Cell* **135**, 1017-1027. doi:10.1016/j.cell.2008.10.022